Universal amplification-free molecular diagnostics by billion-fold hierarchical nanofluidic concentration

Wei Ouyang[a,b] and Jongyoon Han[a,b,c,1]

[a]Department of Electrical Engineering and Computer Science, Massachusetts Institute of Technology, Cambridge, MA 02139; [b]Research Laboratory of Electronics, Massachusetts Institute of Technology, Cambridge, MA 02139; and [c]Department of Biological Engineering, Massachusetts Institute of Technology, Cambridge, MA 02139

Edited by John A. Rogers, Northwestern University, Evanston, IL, and approved July 3, 2019 (received for review March 15, 2019)

Rapid and reliable detection of ultralow-abundance nucleic acids and proteins in complex biological media may greatly advance clinical diagnostics and biotechnology development. Currently, nucleic acid tests rely on enzymatic processes for target amplification (e.g., PCR), which have many inherent issues restricting their implementation in diagnostics. On the other hand, there exist no protein amplification techniques, greatly limiting the development of protein-based diagnosis. We report a universal biomolecule enrichment technique termed hierarchical nanofluidic molecular enrichment system (HOLMES) for amplification-free molecular diagnostics using massively paralleled and hierarchically cascaded nanofluidic concentrators. HOLMES achieves billion-fold enrichment of both nucleic acids and proteins within 30 min, which not only overcomes many inherent issues of nucleic acid amplification but also provides unprecedented enrichment performance for protein analysis. HOLMES features the ability to selectively enrich target biomolecules and simultaneously deplete nontargets directly in complex crude samples, thereby enormously enhancing the signal-to-noise ratio of detection. We demonstrate the direct detection of attomolar nucleic acids in urine and serum within 35 min and HIV p24 protein in serum within 60 min. The performance of HOLMES is comparable to that of nucleic acid amplification tests and near million-fold improvement over standard enzyme-linked immunosorbent assay (ELISA) for protein detection, being much simpler and faster in both applications. We additionally measured human cardiac troponin I protein in 9 human plasma samples, and showed excellent agreement with ELISA and detection below the limit of ELISA. HOLMES is in an unparalleled position to unleash the potential of protein-based diagnosis.

molecular diagnostics | microfluidics | electrokinetics | nucleic acid | protein

Disease diagnosis based on the detection of ultralow-abundance molecular biomarkers is of enormous promise (1–3). Subfemtomolar to attomolar detection sensitivity is often required in clinical diagnostics (4), a regime where only single-digit to hundreds of target biomolecules exist in a typical sample volume of ~10 μL. It has been well recognized that, with the advancement of micro/nanoscale biosensors, detection of ultralow-abundance biomarkers is no longer limited by the intrinsic sensitivity of biosensors, but by the slow mass transport and weak reaction kinetics in such highly diluted solutions (5–7). Due to these fundamental limits, the majority of biosensors could only directly detect picomolar to femtomolar target biomolecules (8–10). Recently, subfemtomolar sensitivity was reported for several nanomaterials- and nanostructures-based biosensors, which, however, still required long incubation time (several hours to over a day) (11–14) and/or have not been validated in real biofluids (5, 14).

To date, chemical amplification of target molecules or detection signals remains the paradigm for biomarker detection in clinical diagnostics (1). Disease-marking nucleic acids are routinely amplified by PCR or other enzymatic processes before being detectable (4, 15, 16). Despite their unprecedented amplification power, nucleic acid amplification techniques inherently suffer from issues of enzyme instability and variety, nonspecific amplification, amplification errors and biases, and poor multiplex ability, as well as practical issues of speed, cost, the tedious and stringent sample preparation, and dependence on instruments and trained personnel, to different degrees (17, 18). These limitations restrict the realization of simple and reliable nucleic acid tests, especially for home, clinics, and other resource-limited settings. On the other hand, there exist no amplification processes that can replicate proteins, rendering protein-based diagnosis severely lagging behind. Nowadays, protein detection relies on signal amplification processes following the occurrence of target–probe binding, which remains limited by the slow mass transport and weak binding kinetics at ultralow target concentrations. Consequently, the gold standard enzyme-linked immunosorbent assay (ELISA) could only routinely detect picomolar concentrations, far above the subfemtomolar concentrations of many protein biomarkers (3). Although advanced signal amplification assays enabled subfemtomolar detection of proteins, they typically require many steps and take several hours to over a day (11, 12, 19). Taken together, novel molecular enrichment techniques that are as powerful as PCR, yet fast, simple, robust, and, most critically, universal for both nucleic acids and proteins, would revolutionize the field of molecular diagnostics and many relevant fields of biological science and engineering.

In the past 2 decades, a number of microfluidic techniques have been developed for biomolecule enrichment, such as field amplified sample stacking (20), isoelectric focusing (21), electric field gradient focusing (22), dielectrophoretic trapping (23), isotachophoresis (24), and electrokinetic trapping (25). Being physical methods, microfluidic enrichment techniques are naturally immune to the issues of chemical amplification and are applicable to both nucleic acids and proteins. However, despite the significant efforts on improving the enrichment performance by optimization

Significance

The need for accurate analysis of low-abundance nucleic acids and proteins is ubiquitous in biological science and engineering. The revolutionary nucleic acid amplification techniques enabled single-copy detection of nucleic acids but have many issues restricting their implementation in diagnostics and various applications. Protein analysis lags severely behind because there are no protein amplification techniques. We report a universal technique that unprecedentedly achieves billion-fold enrichment of both nucleic acids and proteins directly in complex biological samples, which may play an enabling role in the rapid analysis of ultralow-abundance biomolecules (especially proteins) in many fields. We demonstrate direct detection of attomolar nucleic acid and protein biomarkers in crude clinical samples within an hour, validating its generic functionality in clinical diagnostics.

Author contributions: W.O. and J.H. designed research; W.O. performed research; W.O. analyzed data; and W.O. and J.H. wrote the paper.

The authors declare no conflict of interest.

This article is a PNAS Direct Submission.

[1]To whom correspondence may be addressed. Email: jyhan@mit.edu.

This article contains supporting information online at www.pnas.org/lookup/suppl/doi:10.1073/pnas.1904513116/-/DCSupplemental.

Published online July 29, 2019.

of experimental conditions, operation protocols, and device design (24, 26, 27), existing microfluidic enrichment techniques could achieve only 10^2- to 10^6-fold enrichment of biomolecules in an hour (24, 26), which is essentially limited by the small sample volumes (approximately microliters) microfluidic devices can process in a reasonable amount of time (considering mass conservation). With performance far below that of PCR, existing microfluidic enrichment techniques cannot meet the needs of clinical diagnostics. Here, we report a hierarchical nanofluidic molecular enrichment system (HOLMES) that is capable of achieving billion-fold enrichment of biomolecules within 30 min. Unlike previous works that focused on the optimization of individual concentrators, we propose the paradigm of hierarchical concentration, in which massively parallel nanofluidic concentrators are simultaneously operated to concentrate biomolecules from milliliters of samples, and subsequently the concentrated biomolecules are reconcentrated into a single microfluidic zone by hierarchical cascading structures, thereby dramatically increasing the concentration throughput and speed. Besides its record-breaking performance that far exceeds conventional techniques, HOLMES also remarkably features the ability to selectively enrich target biomolecules and simultaneously deplete nontargets directly from raw clinical samples, thereby enormously increasing the signal-to-noise ratio of detection. Furthermore, HOLMES is fabricated by the low-cost polydimethylsiloxane (PDMS) and operated simply by DC voltages and gravitational flows, making it ideal for point-of-care settings. By integration with fluorescence-based assays, we demonstrate that HOLMES can enhance the performance of conventional assays to enable the direct detection of various nucleic acids and proteins from clinical samples down to the attomolar range within an hour, validating the universal functionality of HOLMES in clinical diagnostics.

Principle and Design of HOLMES

HOLMES has a hierarchical architecture with vertically stacked massively parallel microchannels in the first stage and a single microchannel in the final stage, between which the numbers of microchannels are scaled down by 10- to 100-fold per stage (Fig. 1*A*). Each stage has an input port from the main inlet or prior stage, an output port to the latter stage or final outlet, and valved side outlets. Within each stage, a perpendicularly patterned nanochannel network bridges the parallel microchannels and side buffer channels at the bottom. The nanochannel network is made by the cation-selective membrane Nafion [pore diameter, ∼4 nm (28)] in this work to enrich negatively charged biomolecules (nucleic acids and most proteins at the neutral pH). Positively charged biomolecules can be enriched by use of anion-selective membranes. When a stage is activated, the input is biased to a positive DC voltage (V), the side outlet(s) are opened and grounded (G), and the buffer channels are grounded (G) (Fig. 1*B*).

Under this configuration, a tangential electric field (E_T) is induced along the microchannels, and a normal electric field (E_N) is induced along the Nafion nanochannel network. Driven by E_N, cations in the microchannels are preferentially transported through the highly conductive cation-selective nanochannel network to the buffer channels, inducing ion depletion zones with significantly amplified electric fields near the microchannel junctions (Fig. 1*B*) (29). Meanwhile, under E_T, biomolecules enter the microchannels with the fluid flow induced by the electric field (electroosmosis [EO]) but are also subject to counter-directional electric force (electrophoresis [EP]), which is proportional to the magnitude of the electric field. As biomolecules enter the ion depletion zones, the electrophoretic velocity grows as strong as the electroosmotic velocity (net velocity becomes zero), resulting in the electrokinetic trapping of biomolecules (Fig. 1*B*). Accompanying the continuous electroosmotic injection of samples into the microchannels, biomolecules become concentrated at the trapping points (29, 30). Biomolecules concentrated in massive parallel microchannels are released and reconcentrated into the second stage with fewer microchannels by closing the side outlets of the first stage and opening those of the second stage (Fig. 1*C* and *SI Appendix*, section 1), which is repeated stage by stage until biomolecules are reconcentrated into the single microchannel in the final stage. Through reconcentration, the concentration performance is dramatically increased.

We designed devices with different enrichment capacities to suit the needs of various applications (Fig. 2*A*). The 640- (Fig. 2*B*), 3,200- (Fig. 2*C*), and 38,400-plex (Fig. 2*D*) devices comprise 64, 320, and 3,840 channels of 200 μm in width in the first stage and a single channel of 20 μm in width in the final stage (all channels are 15 μm deep), with equivalent channel width ratios of 640, 3,200, and 38,400, respectively. The 640-, 3,200-, and 38,400-plex devices can concentrate biomolecules from ∼0.2, ∼1.0, and ∼10.0 mL of samples in 0.1× PBS in 15 min in the first stage, respectively, which ultimately converge into a concentration zone (∼10 pL) in the final stage. Based on mass conservation, one could expect concentration of biomolecules by 10^7-, 10^8-, and 10^9-fold, respectively. The 38,400-plex device consists of 12 plasma-bonded PDMS layers in the first stage to accommodate all of the microchannels (Fig. 2*E* and *SI Appendix*, section 2). The devices were operated at an electric field of 80 to 200 V/cm to achieve rapid and efficient concentration of biomolecules (*SI Appendix*, section 3). During the transfer of biomolecules between stages, gravitational flows were superposed on the electroosmotic flows to increase the flow rates by adjustment of the heights of the outlet tubings (*SI Appendix*, section 4).

Enrichment Performance of HOLMES

We visualized the workflow of HOLMES with 10 pM fluorescently labeled single-stranded DNA (ssDNA) in 0.1× PBS. The ssDNA formed concentration plugs in the massively parallel microchannels in the first stage following 15 min of concentration (Fig. 3*A*). The peak fluorescence intensities of the concentration plugs were increased stage by stage through reconcentration, resulting in a 4–order-of-magnitude boost from the first to the final stage of the 38,400-plex device (Fig. 3*B*).

We evaluated the concentration factors (ratio of peak concentration to initial concentration) achieved by HOLMES using ssDNA in 0.1× PBS with initial concentrations from 10^{-10} to 10^{-17} M. The fluorescence intensities of the concentration plugs increased with time as concentration proceeded (Fig. 4 *A*–*C*). While concentration plugs could only be observed for initial concentrations no less than 1 pM in the first stage (using conventional fluorescence microscopy), the reconcentration steps gradually lowered the detection limits, which were 1000, 100, and 10 aM at the final stages of the 640-, 3,200-, and 38,400-plex devices, respectively. By translating the fluorescence intensities to ssDNA concentrations using a standard curve (*SI Appendix*, section 5), we calculated the concentration factors at all stages (Fig. 4 *D*–*F*). The concentration factor in the first stage was $\sim 10^4$ at 1 pM, which is higher (near 10^5) for lower initial concentrations according to previous studies (not directly observable by the microscope used) (31, 32). Subsequent reconcentrations boosted the concentration factors by $\sim 3 \times 10^2$-, 10^3-, and 10^4-fold in the 640-, 3,200-, and 38,400-plex devices (Fig. 4 *D*–*F*), leading to record-breaking maximum concentration factors of 0.76×10^7, 0.73×10^8, and 0.55×10^9 within 30 min, respectively. Tests with BSA suggest comparable concentration performance on proteins (*SI Appendix*, section 6).

We then amplified DNA solutions by the gold standard qPCR (amplicon length, 96 bp), which detected 10 aM as HOLMES did but took much longer time (75 vs. 30 min) (Fig. 4*G*). It is noteworthy that qPCR showed false positive in the no-template control because of nonspecific amplification, while HOLMES was naturally immune to this problem as a nonamplification method. Furthermore, given the same total run time (not even counting the lengthy sample preparation time of qPCR), we compared the amplification/concentration factors of the 2 techniques (Fig. 4*H*). We calculated the amplification factor of qPCR based on ideal exponential duplication, and the concentration factor of HOLMES by varying the concentration time of the first stage and fixing the reconcentration protocol in the latter stages (*SI Appendix*, section 7). Overall, even excluding the sample preparation time of qPCR, HOLMES is still more efficient than qPCR, where as high as billion-fold enrichment of nucleic

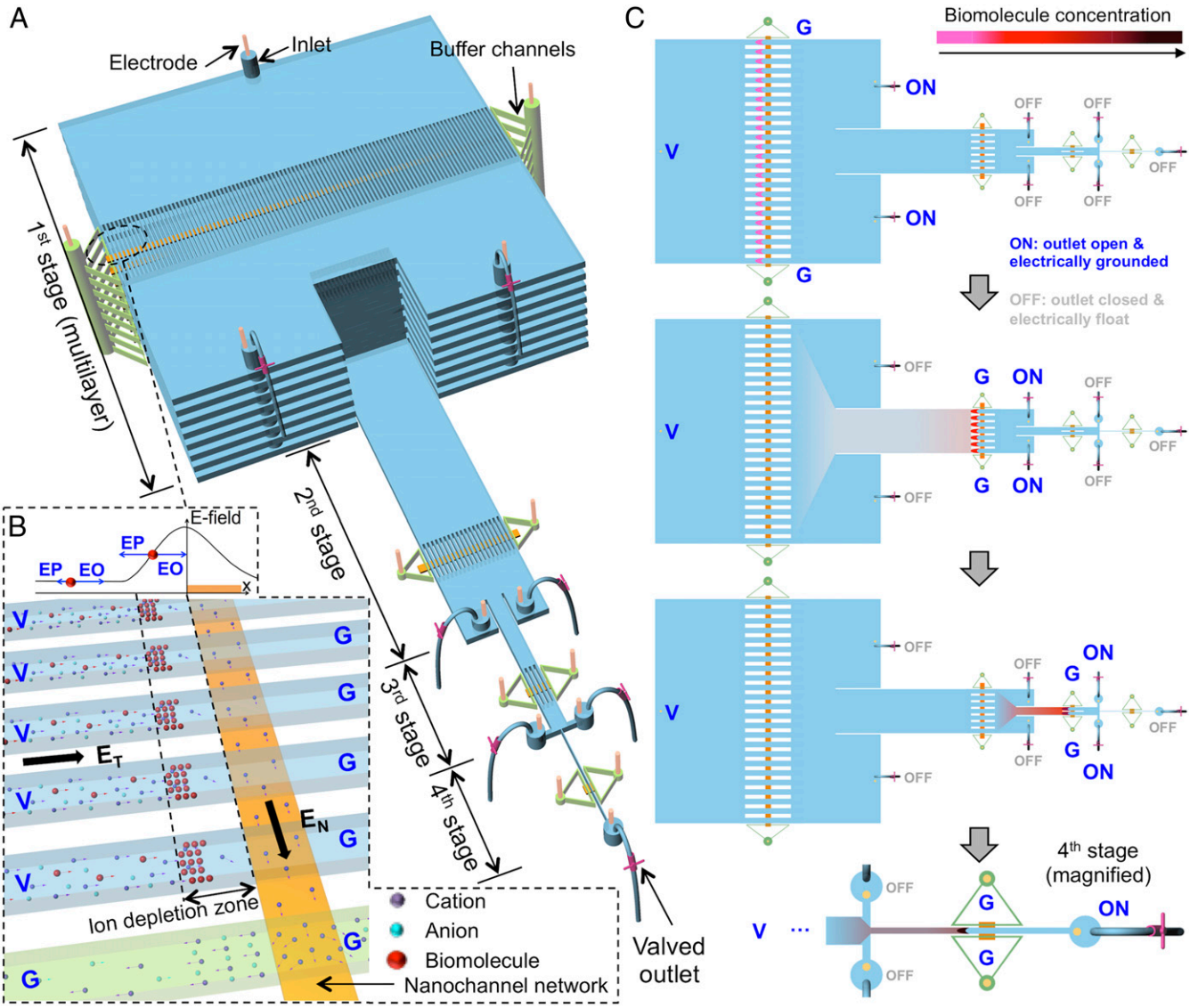

Fig. 1. Principle of HOLMES. (*A*) Schematic of HOLMES with hierarchical multistages. At each stage, parallel microchannels and buffer channels are bridged by a thin nanochannel network patterned on the bottom of the microchannels. (*B*) Schematic of nanofluidic biomolecule concentration in massively parallel channels. Under the electrical configuration shown, biomolecules are electroosmotically injected into the parallel channels and electrokinetically concentrated in the ion depletion zones induced near the micronanochannel junctions. (*C*) Schematic of relayed reconcentration of biomolecules from massively parallel microchannels into a single microchannel to dramatically boost the concentration performance.

acids is needed. However, more crucially, HOLMES works on proteins, while PCR does not.

Nucleic Acid Detection by HOLMES

We went on to demonstrate that HOLMES could maintain high-concentration performance in clinical samples and enable the detection of ultralow-abundance molecular biomarkers. In clinical samples, the much more abundant cell-free DNAs [e.g., ~100 ng/mL in human serum (33)] and proteins [e.g., ~100 mg/mL in human serum (34)] would present significant noises for the sensitive and specific detection of targets and also suppress the concentration of targets (*SI Appendix*, section 8). HOLMES uses affinity probes to recognize the targets and modulate their electrophoretic mobility, which enables the selective enrichment of targets and simultaneous depletion of interfering background biomolecules.

In nucleic acid detection, we used a fluorescently labeled complementary peptide nucleic acid (PNA) probe, which is a charge-neutral DNA analog with higher affinity and specificity (even capable of distinguishing single-base mismatch) (35, 36). The electrophoretic mobility of the hybridized DNA–PNA is between that of the background DNAs and proteins (Fig. 5*A*). The charge-neutral PNA probe is not subject to electric forces and hence directly passes the electric field barrier without being concentrated (not manifesting fluorescence), while the negatively charged DNA–PNA complex is concentrated (Fig. 5*A*, *Left*), the fluorescence of which quantifies the concentration of the target DNA.

As previously mentioned, negatively charged biomolecules are concentrated where electrophoresis (velocity $\propto \mu \cdot E$; μ is electrophoretic mobility; E is electric field) and electroosmosis are balanced. Because of the different mobility, the background DNAs, DNA–PNA complex, and background proteins form separate concentration zones within the electric field barrier, with background proteins closest to the peak of the electric field barrier (Fig. 5*A*, *Left*). By imposition of appropriate additional fluid drag force on the biomolecules with a pressure-driven flow (specifically, gravitational flow [GF] in this work), the total fluid

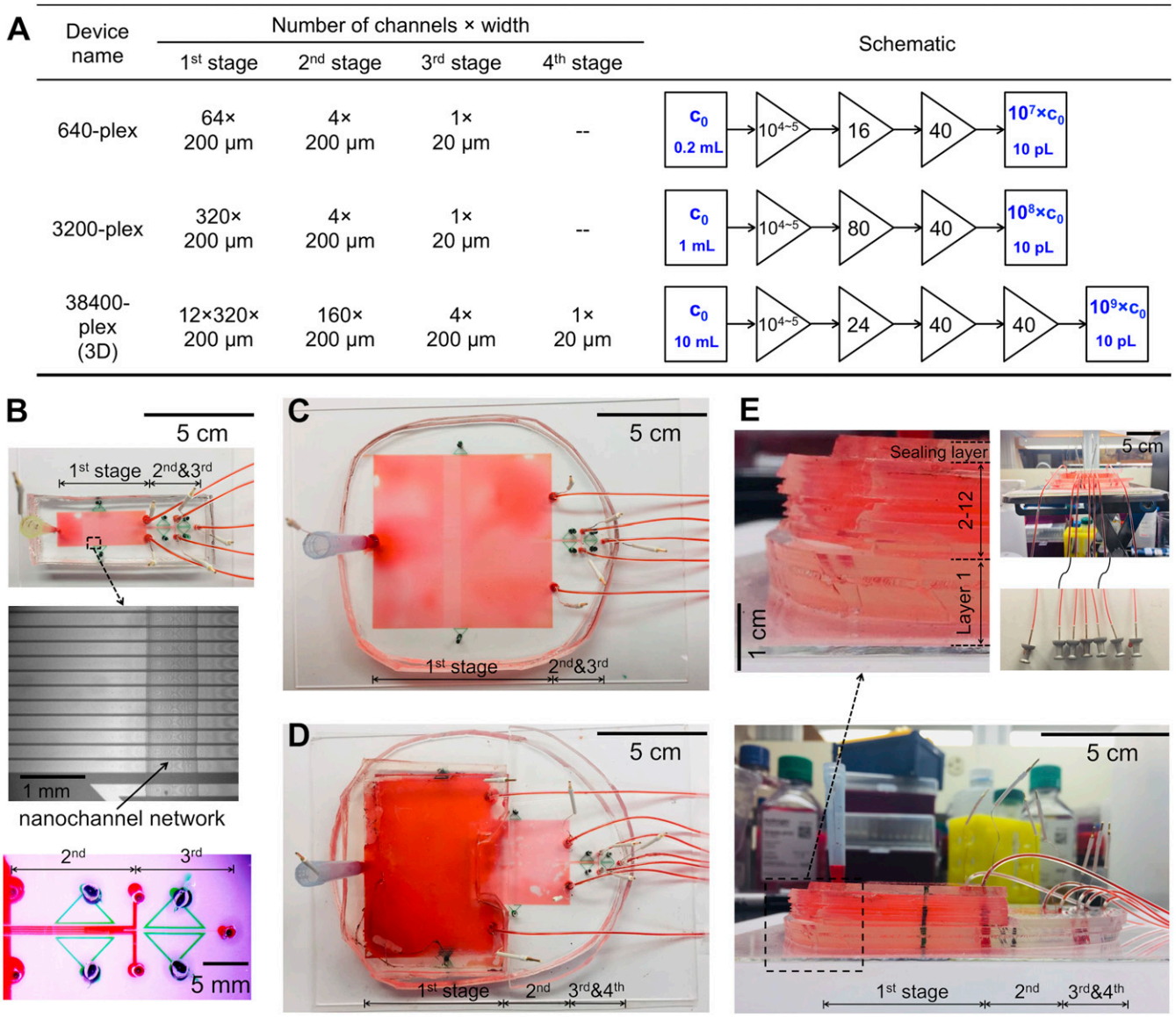

Fig. 2. Design of HOLMES devices. (*A*) The dimensions of the 640-, 3,200-, and 38,400-plex devices. The 640-, 3,200-, and 38,400-plex devices can concentrate biomolecules from 0.2, 1.0, 10.0 mL of samples (15 mM ion concentration) into a concentration zone of ~10 pL, corresponding to concentration factors of 10^7, 10^8, and 10^9 based on mass conservation, respectively. (*B*) Photo of the 640-plex device fabricated by PDMS, micrograph of the first stage, and magnified view of the second and third stages. (*C*) Photo of the 32,000-plex device. (*D*) Photo of the 38,400-plex device. (*E*) Side view of the 38,400-plex device, magnified view of the vertically stacked multiple layers, and side view of the device showing the tubings of the side outlets turned on and off by the insertion and removal of push pins. In the photos, the devices were loaded with red and green food dye solutions to better visualize the fluidic structures.

drag force (EO+GF) exceeds the maximum electrophoretic force that can be exerted on the background proteins by electric field barrier (at its peak), thereby allowing the escape of the background proteins from the electric field barrier (Fig. 5*A*, *Right*) (37). Meanwhile, the total fluid drag force cannot overcome the maximum electrophoretic effect exerted on the background DNAs and DNA–PNA complex due to their higher mobility, which allows them to remain concentrated (Fig. 5*A*, *Right*) (37). By filtering out the background proteins and concentrating background DNAs in a separate zone, HOLMES could minimize the interference of background biomolecules. We visualized the selective enrichment using multiwavelength fluorescence imaging with 100 ng/mL fluorescently labeled DNA (green peak) and 10 mg/mL BSA (native fluorescence, red peak) in the detection of 1 nM target DNA by PNA (blue peak). The left-panel fluorescence images (Fig. 5*A*) indicate the coconcentration of different species in separate zones, and the right-panel fluorescence image shows the filtration of proteins under an additional gravitational flow.

We demonstrate the detection of a fragment of Mycobacterium *tuberculosis* IS6110 genomic DNA (96 bases long) spiked in various biofluids under the selective enrichment mode (*Materials and Methods* and *SI Appendix*, section 9) (38), with sample-to-answer time of ~35 min. In PBS (Fig. 5 *B–D* and *SI Appendix*, section 10), HOLMES was able to detect 100 aM target DNA from 0.6-mL samples using the 3,200-plex device and 10 aM from 6.5-mL samples using the 38,400-plex device. Urine contains few DNAs and proteins but many intrinsically fluorescent constituents (e.g., flavins, porphyrins, bilirubin) that are weakly charged (39). These low-mobility fluorescent constituents were filtered like proteins, although trace remnants concentrating near the nanochannel network were observed under long exposure time (8000 ms) (Fig. 5 *E–G* and *SI Appendix*, section 10). Nonetheless, HOLMES was able to distinguish 10 aM target DNA in urine,

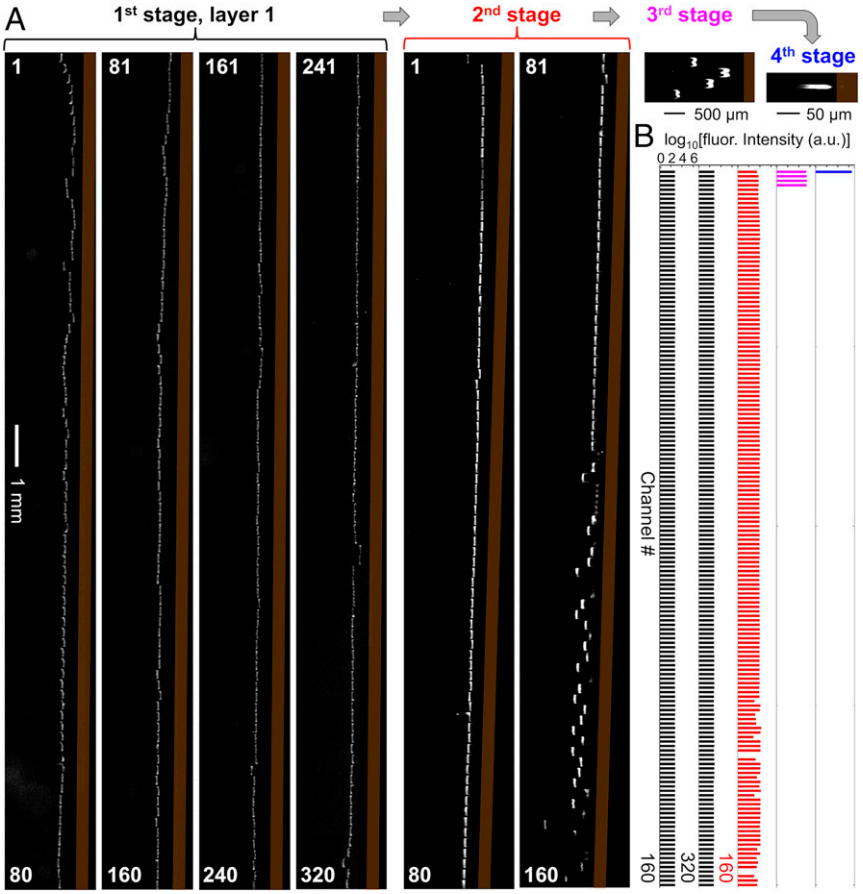

Fig. 3. Working process of HOLMES in a 38,400-plex device. (*A*) The fluorescence images of the ssDNA concentration plugs in the parallel microchannels of different stages. Due to the limited field of view of the microscope, the fluorescence images were taken frame by frame and stitched together. (*B*) The fluorescence intensities of the concentration plugs in individual microchannels of different stages, which increase stage by stage logarithmically.

owing to the minimal interfering biomolecular background of urine. For samples in 0.25× serum (Fig. 5 *H*–*J* and *SI Appendix*, section 10), we similarly observed the fluorescent peak of the DNA–PNA complex and remaining proteins near the nanochannel network. HOLMES was able to directly detect 100 aM target DNA in 0.25× serum.

Protein Detection by HOLMES

Detection of ultralow-abundance protein biomarkers (less than ∼1 fM or $\sim 10^{-4}$ ng/mL) in blood-derived samples below the currently clinically achieved level (∼1 pM or $\sim 10^{-1}$ ng/mL) is of intense interest for the early diagnosis of diseases (4). In protein detection, we used a high-mobility capture antibody (Ab) conjugated by fluorescently labeled ssDNAs (total length, 400 bases) and a capture Ab to capture the target protein, forming a DNA–Ab–target complex with higher mobility than the background proteins (Fig. 6*A*). Based on the mobility difference, the complex (and excess high-mobility capture Ab) could be selectively enriched under a gravitational flow. The selectively concentrated DNA–Ab–target complex was collected onto the surface of a microbead (diameter, 10 μm) via a detection Ab (Fig. 6 *B* and *C*), which functioned as an additional mechanism of molecular enrichment and affinity recognition. After washing out the excess capture Ab, the DNA–Ab–target–Ab sandwiches on the microbead were detected by fluorescence. We investigated the performance of the proposed assay by detecting the HIV p24 protein in the 3,200-plex device, except that the microchannel in the final stage was widened to 100 μm to accommodate the microbead trapping structure. The assay was first performed without target concentration, which had a detection limit of 10 pM both in PBS with 10 mg/mL BSA and 0.25× serum (Fig. 6*D*). With target concentration from ∼0.6-mL samples, fluorescence signals could be detected above the negative control for as low as 10 aM in PBS and 10 to 100 aM in 0.25× serum, which is a nearly 6–order-of-magnitude enhancement over the assay without concentration. Compared with the gold standard ELISA (detection limit, ∼1 pM) (3), HOLMES detected protein concentrations of about 5 orders of magnitude lower with significantly shorter time (60 min vs. several hours to over a day).

Next, we validated the reliability of HOLMES by comparing its results with well-established commercially available ELISA. To enable the direct comparison between HOLMES and ELISA, we chose human cardiac troponin I (cTnI) as the target protein, because the cTnI concentration (picograms per milliliter to approximately nanograms per milliliter) in most patients is close to the detection range of ELISA. Most commercial ELISA kits and other cTnI diagnostics assays have detection limits of 0.01 to 0.1 ng/mL (40), but there is emerging interest in detecting even lower levels of cTnI for early prediction of cardiac diseases (41). As shown in Fig. 6*E* and *SI Appendix*, sections 11 and 12, HOLMES correlated well with ELISA in the range of 0.1 to 10 ng/mL in 6 patients. Moreover, HOLMES was able to detect much lower concentrations of cTnI in 3 patients (as low as ∼0.001 ng/mL) that were not detectable by ELISA. Therefore, HOLMES could significantly advance the capability of protein-based diagnosis.

Biomarker detection from whole blood is the focus of the next-generation molecular diagnostics. By adopting mobility-based selective enrichment demonstrated in this paper, we envision HOLMES can potentially selectively enrich high-mobility biomolecules and remove the low-mobility blood cells to enable direct biomarker detection in whole blood. Additionally, many

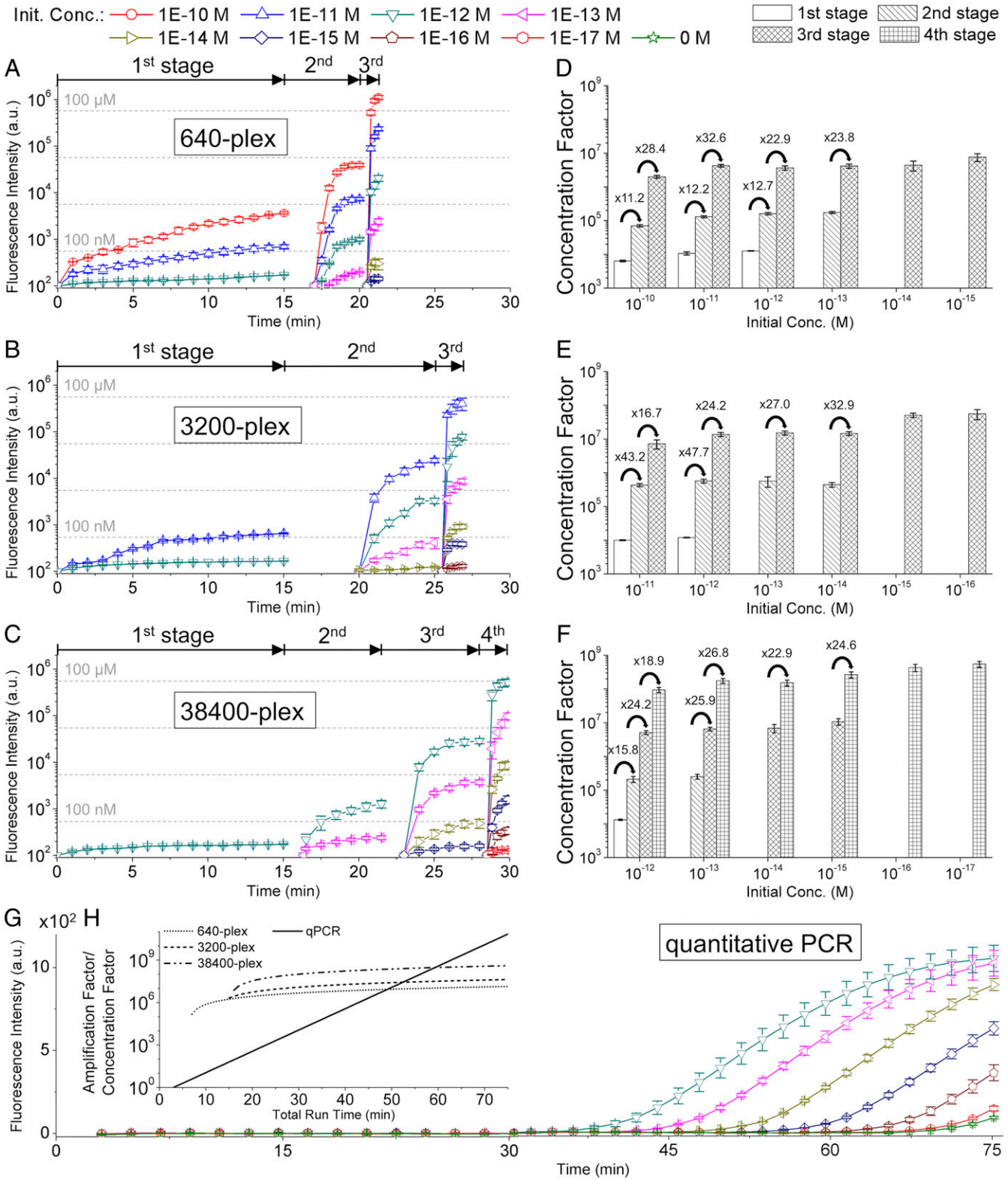

Fig. 4. Enrichment performance of HOLMES. The temporal evolution of the average peak fluorescence intensities of the concentration plugs at the active stages in the (*A*) 640-, (*B*) 3,200-, and (*C*) 38,400-plex devices. Concentration factors at different stages and different initial concentrations in the (*D*) 640-, (*E*) 3,200-, and (*F*) 38,400-plex devices. During experiments, we imaged the microchannels at the center of the corresponding stages in 1 field of view of the microscope (12 microchannels in the first and second stages, and full views of the third and fourth stages). Only imaged microchannels were used for data processing. (*G*) The temporal evolution of fluorescence intensities in qPCR amplifying a DNA of the same initial concentrations (amplicon length, 96 bp). A 2-μL sample is added into 20 μL of reagent mixture for each reaction. (*H*) Comparison of the concentration factor of HOLMES and amplification factor of qPCR. Each data point represents the mean and SD of triplicate runs.

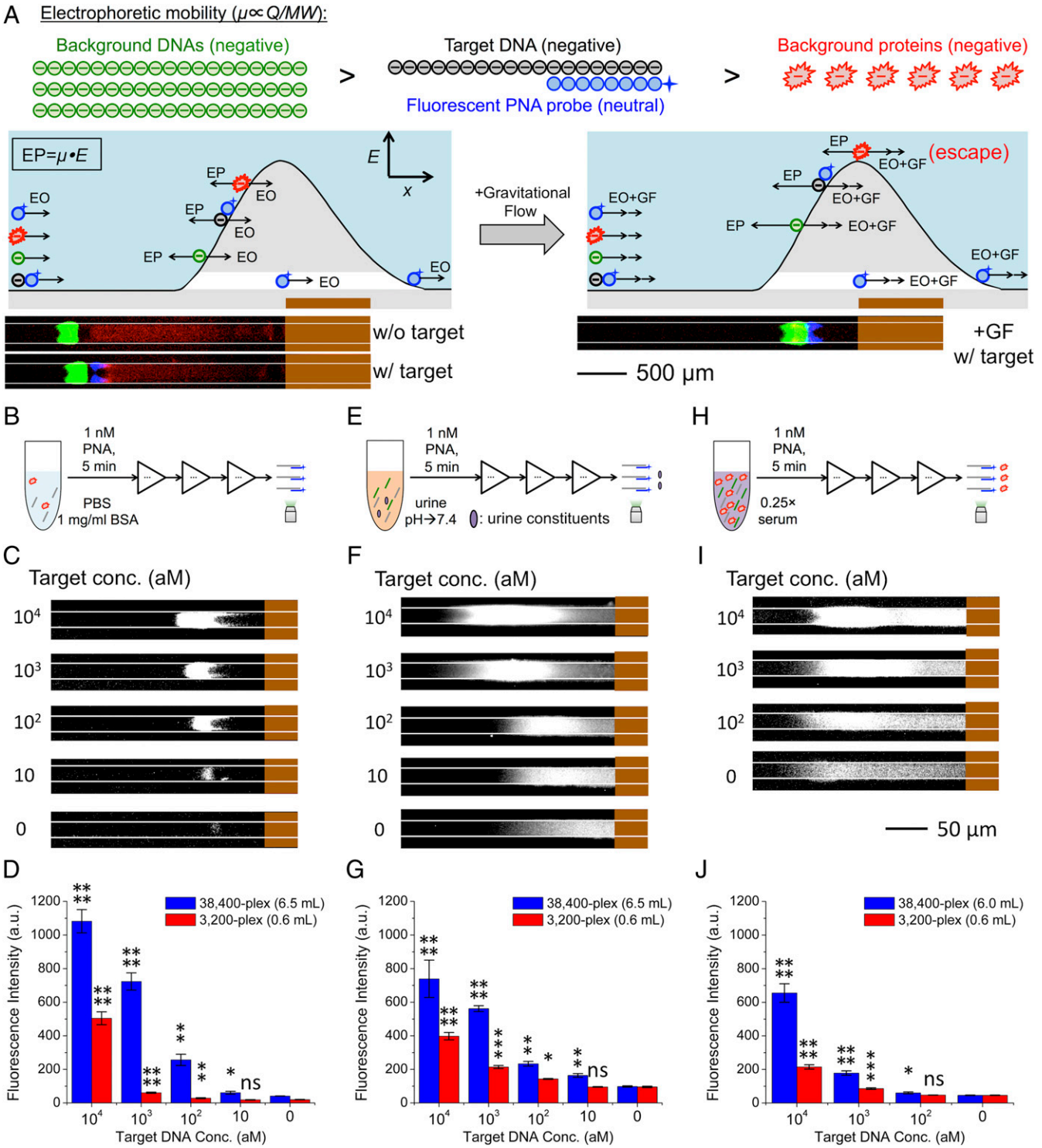

Fig. 5. Nucleic acid detection by HOLMES. (*A*) Schematic of selective nucleic acid enrichment. The concentration behaviors of biomolecules of different electrophoretic mobility within the electric field barrier are illustrated. The addition of gravitational flow enables proteins to escape from the peak of the electric field barrier, thereby not being concentrated. The fluorescence images show concentration of 100 ng/mL fluorescently labeled DNA (green peak) and 10 mg/mL BSA (native fluorescence; red peak) in the detection of 1 nM target DNA by PNA (blue peak) in HOLMES. (*B*) Workflow, (*C*) fluorescence images, and (*D*) corresponding peak fluorescence intensities of DNA detection in PBS. (*E*) Workflow, (*F*) fluorescence images, and (*G*) corresponding peak fluorescence intensities of DNA detection in human urine. (*H*) Workflow, (*I*) fluorescence images, and (*J*) corresponding peak fluorescence intensities of DNA detection in human serum. Each data point represents the mean and SD of triplicate runs. ns, not significant.

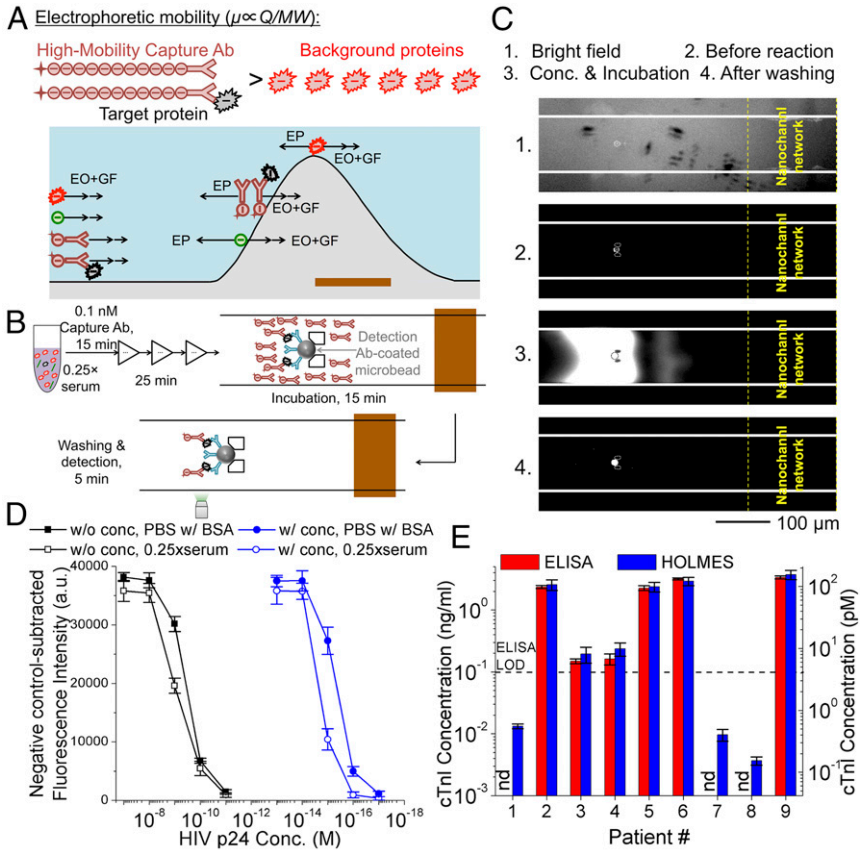

Fig. 6. Protein detection by HOLMES. (*A*) Schematic of selective protein enrichment in HOLMES. (*B*) Schematic and (*C*) micrographs of protein detection by HOLMES. (*D*) Detection of HIV p24 protein by HOLMES. (*E*) Correlation of HOLMES and ELISA in the detection of human cardiac troponin I in patient plasma samples. Each data point represents the mean and SD of triplicate runs. LOD, limit of detection; nd, not detected.

current and emerging methods enable rapid and simple blood cell removal to reduce the interference of the high-density red blood cells (RBCs) on device operation. For example, RBC lysis can be performed on whole blood [taking <1 min using saponin (42)] before it is loaded into the device, after which biomolecules of interest are selectively enriched and protein released from RBCs (hemoglobin) is filtrated by HOLMES (as shown in this paper). Therefore, our system can still be readily applied to whole-blood biomarker detection with minor modification/sample preparation.

Conclusions

In this paper, we have demonstrated that HOLMES achieves billion-fold enrichment of nucleic acids and proteins within 30 min and enables direct detection of attomolar biomolecules in clinical samples within an hour with minimal sample preparation. HOLMES may significantly advance molecular diagnostics in comparison with the state of the art: 1) PCR requires stringent and complex isolation and purification of nucleic acids, and the amplification process is subject to many pitfalls previously mentioned. HOLMES directly enriches nucleic acids in clinical samples by selectively collecting them into a microfluidic space, which greatly simplifies the workflow and avoids many issues of PCR. Remarkably, HOLMES naturally enables unbiased enrichment of multiple sequences, which is very important in nucleic acid studies but highly challenging for PCR. 2) In the domain of protein analysis, HOLMES is in an unparalleled position, which is the only technique providing PCR-comparable performance for proteins. Not being able to amplify proteins, the gold standard ELISA and other signal amplification-based protein assays do not essentially solve the challenges in detecting ultralow-abundance proteins. With unprecedented capability of enriching proteins by billion-fold, HOLMES may unleash rapid and ultrasensitive protein analysis that had not been possible.

We would like to clearly express that we are not competing with the exciting developments of nanoscale biosensors and novel diagnostic platforms like CRISPR-based diagnostics (16), but we are complementary to them. By solving the fundamental problems of slow mass transport and weak reaction kinetics in the detection of ultralow-abundance molecular biomarkers and removing the interfering strong background noises in biofluids, HOLMES can be universally integrated with nanoscale biosensors to significantly enhance their detection sensitivity and improve the speed and statistical reliability of detection. Similarly, for diagnostic platforms like CRISPR that rely on chemical amplification, HOLMES can play an important role in avoiding the common pitfalls of chemical amplification.

We envision this generic and versatile tool could enable rapid identification of bacteria and viruses, early diagnosis of cancer, and various diagnostic applications. HOLMES could also have far-reaching impacts on many fields of biological science and engineering to meet the ubiquitous needs of sensitive and accurate biomolecule analysis, such as genetic studies, sequencing, mass spectrometry, proteomics, and biomarker discovery.

Materials and Methods

Device Fabrication. The device designs were patterned on 6-inch silicon wafers using SU-8 2015 photoresist (MicroChem). The thickness of the SU-8 patterns were ~15 μm. The patterned silicon wafers were treated with trichlorosilane (Sigma-Aldrich) in a vacuum desiccator overnight to prevent adhesion to PDMS. 1) Fabrication of the 640- and 3,200-plex devices. PDMS was poured onto the silicon mold and cured at 65 °C for 3 h. Then the PDMS was peeled off from the silicon mold, and access holes were punched. The Nafion nanochannel networks were patterned on a glass slide by the microflow patterning technique using

Nafion resin (20 wt% solution in lower aliphatic alcohol/H_2O mix; Sigma-Aldrich) (29). Finally, the microchannel-patterned PDMS and the nanochannel network-patterned glass slide were treated with oxygen plasma (Femto Science), and irreversibly bonded under a stereo microscope. 2) Fabrication of the 38,400-plex device. The 38,400-plex device contained a bottom layer with all of the 4 stages and 11 upper layers with only the first stage. The fabrication of the bottom layer was the same as that of the 640- and 3,200-plex devices, except that connecting holes for upper layers were punched at the entrance of the second stage. The 11 upper layers were fabricated separately by the following process: PDMS was poured on the silicon mold and spun-coated at 200 rpm for 1 min (POLOS spin coater 150i), followed by heating at 120 °C for 3 min; the cured PDMS was then peeled off from the silicon mold, which had a thickness of ∼1 mm; access holes and connecting holes to the bottom layers were punched on the PDMS; the nanochannel networks were patterned on a transparent silicone sheet (0.01 inch thick; Green Rubbers Company) by the microflow patterning technique; the microchannel-patterned PDMS was bonded with the nanochannel network-patterned silicone sheet by oxygen plasma. After fabrication of the 11 layers, they were bonded onto the bottom layer one by one by oxygen plasma. The use of the silicone sheets provided strong bonding between the PDMS layers. After fabrication of the devices, pellet Ag/AgCl electrodes (A-M Systems) were inserted into all of the reservoirs and Tygon non-DEHP microbore tubings were inserted into the outlets. Next, a sealing PDMS layer was bonded to the devices to seal the outlets. Finally, uncured PDMS was poured on the sealing layers near the electrodes and tubings as glue, followed by baking at 65 °C for 1 h to form tight sealing.

Device Operation. Before all of the experiments, the devices were passivated with 10 mg/mL BSA in PBS for 10 min and then flushed by PBS to prevent nonspecific binding of biomolecules to the PDMS. A 22-base ssDNA (GTA GGC GAA CCC TGC CCA GGT C, labeled by Alexa Fluor 647 at 5′) synthesized by Integrated DNA Technologies was used to characterize the enrichment performance of HOLMES on nucleic acids. BSA (Sigma-Aldrich) home-labeled by Alexa Fluor 555 was used to characterize the enrichment performance of HOLMES on proteins. The voltages at the inlet, buffer channels, and outlets were applied by a DC voltage source (Stanford Research Systems) via a homemade voltage splitter. The gravitational flows were applied by controlling the hydrostatic pressures through adjusting the heights of the tubings. When a stage was in active concentration mode, its outlets were turned on and electrically grounded, and the corresponding buffer channels were electrically grounded; in other inactive stages, outlets were turned off and electrically floated, and the corresponding buffer channels were electrically floated. The operation flow was as follows: concentration at the first stage, fast transfer of concentrated biomolecules to the entrance of the second stage by gravitational flow and electroosmosis, reconcentration at the second stage, and repeat until biomolecules were reconcentrated at the final stage. The operation sequences of the 3 devices were as follows: 1) 640-plex device: (first, 320 V, 0 Pa, 15 min), (transfer, 200 V, 1500 Pa, 2 min), (second, 200 V, 0 Pa, 3 min), (transfer, 200 V, 1,500 Pa, 0.5 min), (third, 200 V, 0 Pa, 1 min); 2) 3,200-plex device: (first, 640 V, 0 Pa, 15 min), (transfer, 200 V, 5,000 Pa, 5 min), (second, 200 V, 0 Pa, 5 min), (transfer, 200 V, 1,500 Pa, 0.5 min), (third, 200 V, 0 Pa, 1 min); 3) 38,400-plex device: (first, 450 V, 0 Pa, 15 min), (transfer, 360 V, 5,000 Pa, 1.5 min), (second, 360 V, 0 Pa, 5 min), (transfer, 200 V, 5,000 Pa, 1.5 min), (third, 200 V, 0 Pa, 5 min), (transfer, 200 V, 1,500 Pa, 0.5 min), and (fourth, 200 V, 0 Pa, 1 min).

Fluorescence Imaging and Data Analysis. Fluorescence images were acquired using an inverted fluorescence microscope (IX71; Olympus) and a charge-coupled device (CCD) camera (Sensicam qe; Cooke Corporation). A mechanical shutter was used to reduce the photobleaching effect, which was synchronized with the CCD camera by Micromanager. The fluorescence images were analyzed by ImageJ. Because the pixel intensities of the fluorescence images had a range of 0 to 4,095, which could only quantify fluorophore concentrations of 3 orders of magnitude. To quantify the 9–order-of-magnitude concentrations without pixel saturation, we used 10-, 100-, 1,000-, and 8,000-ms exposure times depending on the concentrations of the fluorophores. In the processing of each image, after subtraction of the dark pixel intensity, the fluorescence intensity was normalized to an exposure time of 8,000 ms based on the linear relationship between fluorescence intensity and exposure time (43). Finally, to facilitate log-scale plotting, we added 100 a.u. to the fluorescence intensities of all data of log-scale plots.

qPCR. The 5′ nuclease qPCR assay was used. All of the DNAs and reagents were ordered from Integrated DNA Technologies. The template was a 210-bp dsDNA with the sequence of CTG ATC CGG CCA CAG CCC GTC CCG CCG ATC TCG TCC AGC GCC GCT TCG GAC CAC CAG CAC CTA ACC GGC TGT GGG TAG CAG ACC TCA CCT ATG TGT CGA CCT GGG CAG GGT TCG CCT ACG TGG CCT TTG TCA CCG ACG CCT ACG CTC GCA GGA TCC TGG GCT GGC GGG TCG CTT CCA CGA TGG CCA CCT CCA TGG TCC TCG ACG CGA TCG. The sequences of the forward and reverse primers were GGACCACCAGCACCTAAC and GTAGGCGTCGGTGACAAA, respectively. The sequence of the probe was /6-FAM/TGT GGG TAG/ZEN/CAG ACC TCA CCT ATG T/IABkFQ/, which was labeled by 6-FAM dye at 5′, ZEN quencher in the middle, and IABkFQ quencher at 3′. The amplicon length was 96 bp. Each reaction was performed in 20 μL containing 500 nM primers, 250 nM probe, 1× MasterMix, and 2 μL of template DNA solution. Each concentration of the template DNA was amplified in triplicates. The qPCR was performed with the Bio-Rad C1000 Thermal Cycler. The program of thermal cycling is 3-min initial heating, followed by 40 cycles of 16-s temperature ramp-up, 15-s denaturation at 95 °C, 16-s temperature ramp-down, 60-s annealing and extension, and 10-s plate reading.

Selective Enrichment Mode. The operation protocols of the selective concentration mode were the same as those described in *Device Operation*, except that gravitational flows were also added in the concentration steps to "push" proteins across the electric field barrier. The operation sequences of the 3 devices under the selective concentration mode were as follows: 1) 640-plex device: (first, 320 V, 450 Pa, 15 min), (transfer, 200 V, 1,500 Pa, 2 min), (second, 200 V, 300 Pa, 3 min), (transfer, 200 V, 1,500 Pa, 0.5 min), (third, 200 V, 240 Pa, 1 min); 2) 3,200-plex device: (first, 640 V, 900 Pa, 15 min), (transfer, 200 V, 5,000 Pa, 5 min), (second, 200 V, 300 Pa, 5 min), (transfer, 200 V, 1,500 Pa, 0.5 min), (third, 200 V, 240 Pa, 1 min); 3) 38,400-plex device: (first, 450 V, 600 Pa, 15 min), (transfer, 360 V, 5,000 Pa, 1.5 min), (second, 360 V, 500 Pa, 5 min), (transfer, 200 V, 5,000 Pa, 1.5 min), (third, 200 V, 315 Pa, 5 min), (transfer, 200 V, 1,500 Pa, 0.5 min), and (fourth, 200 V, 290 Pa, 1 min). Due to the high viscosity of serum, the hydrostatic pressures were increased for selective enrichment in serum: 1) 640-plex device: (first, 320 V, 550 Pa, 15 min), (transfer, 200 V, 1,800 Pa, 2 min), (second, 200 V, 375 Pa, 3 min), (transfer, 200 V, 1,800 Pa, 0.5 min), (third, 200 V, 300 Pa, 1 min); 2) 3,200-plex device: (first, 640 V, 11,000 Pa, 15 min), (transfer, 200 V, 6,000 Pa, 5 min), (second, 200 V, 375 Pa, 5 min), (transfer, 200 V, 1,800 Pa, 0.5 min), (third, 200 V, 300 Pa, 1 min); 3) 38,400-plex device: (first, 450 V, 750 Pa, 15 min), (transfer, 360 V, 6,000 Pa, 1.5 min), (second, 360 V, 625 Pa, 5 min), (transfer, 200 V, 6,000 Pa, 1.5 min), (third, 200 V, 400 Pa, 5 min), (transfer, 200 V, 1,800 Pa, 0.5 min), and (fourth, 200 V, 330 Pa, 1 min).

Nucleic Acid Detection. The sequence of the target DNA was CGA GCG TAG GCG TCG GTG ACA AAG GCC ACG TAG GCG AAC CCT GCC CAG GTC GAC ACA TAG GTG AGG TCT GCT ACC CAC AGC CGG TTA GGT GCT GGT (Integrated DNA Technologies). The sequence of the PNA probe was TCA CCT ATG TGT CGA ACT GG with 5′ labeled by Cy5 dye (PNA Bio). Pooled human urine was ordered from Lee BioSolutions. The pH of the urine was adjusted to 7.4 using 1 M sodium hydroxide (Sigma-Aldrich). Human serum was ordered from Millipore Sigma. Different concentrations of the target DNA were spiked into PBS with 10 mg/mL BSA, urine, and 0.25× serum (diluted by PBS). The PNA probe was added to the samples to a final concentration of 1 nM, followed by 5-min incubation. Next, the samples were processed by the devices under the selective concentration mode, which took about 30 min. Finally, fluorescence images of the microchannels of the final stages were taken and analyzed. Each sample was tested 3 times using 3 devices.

DNA–Antibody Conjugation. The ssDNA was 96 bases long with the sequence of AGC TAG CTA GCT AGC TAG CTA GCT AGC TAG CTA GCT AGC TAG CTA GCT AGC TAG CTA GCT AGC TAG CTA GCT AGC TAG CTA GCT AGC TAG CTA GCT, which was labeled with an amine group at 5′ and a 6-FAM dye at 3′. The manufacturer of the capture Ab is described in *Protein Detection*. The conjugation kit was ordered from SoluLink. Basically, the amine-DNA was modified with succinimidyl-4-formylbenzamide (S-4FB) cross-linker, and the capture Ab was modified with succinimidyl 6-hydrazinonicotinate acetone hydrazone (S-HyNic) cross-linker, which were finally linked by the cross-linker pair. The DNA was resuspended to a concentration of 0.5 OD_{260}/μL, mixed with S-4FB at a 1:20 molar ratio, and incubated for 2 h. The mixture was purified with the Zeba desalting column (Thermo Fisher Scientific) 3 times to remove excess free S-4FB. The capture Ab was reconstituted to 1 mg/mL in PBS, mixed with S-HyNic at a 1:20 molar ratio, and incubated for 2.5 h. The mixture was purified with the Zeba desalting column 3 times to remove excess free S-HyNic. The S-HyNic–modified Ab and S-4FB–modified DNA were mixed at a molar ratio of 1:7. A 1/10 volume of TurboLink catalyst (SoluLink) was added to the mixture. The mixture was then incubated overnight. Finally, the mixture was purified to remove excess DNA and exchanged to PBS buffer using the Zeba desalting column. The resulted DNA–Ab conjugate contained approximately 4 DNA molecules on 1 Ab molecule.

Microbead Functionalization and Trapping. The SuperAvidin-coated microbead (10 μm in diameter) was ordered from Bangs Laboratory. The manufacturer of the detection Ab is described in *Protein Detection*. A 5-μL microbead suspension

(10 mg/mL) was washed in PBS 3 times by centrifugation at 2,500 × *g* for 5 min. The detection Ab was biotinylated with EZ-Link NHS-PEG4-Biotin (Thermo Fisher Scientific). A volume of 10 μL of 1 mg/mL biotinylated Ab was mixed with the washed microbeads and incubated on a rotator for 15 min at room temperature. Finally, the microbeads were washed in PBS 5 times by centrifugation at 2,500 × *g* for 5 min to remove excess antibodies. The Ab-coated microbead suspension was stored at 1 mg/mL at 4 °C and used within 3 d. Upon experiments, 2-μL microbead suspension was diluted by 1,000 times in PBS. The diluted microbead suspension was pipetted into the microchannel of the final stage through the final outlet. Then a syringe was used to suck the microbead suspension back to the final outlet, during which the microbeads backflowed and one microbead became trapped between the PDMS pillars. Finally, PBS was loaded into the device through the main inlet to wash excess microbeads remaining in the final stage.

Protein Detection. The HIV p24 Ab pair and recombinant HIV p24 protein were from the HIV-1 Gag p24 DuoSet ELISA kit (R&D Systems). The Magic human cTnI Ab pair (Creative Diagnostics) was used for the detection of cTnI (clone TPC102 as the capture Ab and clone TPC110 as the detection Ab). Recombinant human cTnI protein was ordered from Abcam. 1) HIV p24 detection: Different concentrations of recombinant HIV p24 protein were spiked into PBS with 10 mg/mL BSA and 0.25× serum (diluted by PBS). The DNA-conjugated high-mobility capture Ab was added to the samples to a final concentration of 0.1 nM, followed by 15-min incubation. Next, the samples were processed by the 3,200-plex device under the selective concentration mode, which took about 25 min. The DNA–capture Ab–p24 complex was concentrated in a region trapped with a detection Ab-coated microbead. The voltage was turned off and the final outlet was turned off, such that the concentration plug remained in the microbead-trapped region. After 15 min of incubation, the final outlet was turned on and the concentration plug was washed out. Finally, fluorescence images of the microbead were taken and analyzed. Each sample was tested 3 times using 3 devices. 2) cTnI detection: The standard curve of cTnI detection in the 3,200-plex device was established following the same protocol as HIV p24 detection. The 9 patient plasma samples for cTnI detection were deidentified diagnostic remnants ordered from Discovery Life Sciences, which were collected through Department of Health and Human Services/Office for Human Research Protections- and Health Insurance Portability and Accountability Act of 1996-compliant practices.

ELISA. All of the materials and reagents (except antibodies and protein standard) were from the DuoSet Ancillary Reagent Kit 2 (R&D Systems). The reagent diluent was PBS with 10 mg/mL BSA and 0.2% Triton X-100. The washing buffer was PBS with 0.05% Tween 20. The working concentration of the capture Ab was 2 μg/mL in PBS. The working concentration of the detection Ab was 100 ng/mL in reagent diluent. The samples were diluted by four times in the reagent diluent. A volume of 100 μL of capture Ab solution was loaded into each well of the 96-well microplate and incubated overnight at room temperature. Then each well was washed with 400 μL of washing buffer for 3 times, followed by blocking with 300 μL of reagent diluent for 1 h. After washing of the microplate as previously mentioned, 100 μL of sample or standard solution was loaded into each well, and incubated for 2 h. After washing, 100 μL of detection Ab solution was loaded into each well and incubated 2 h at room temperature. After washing, 100 μL of streptavidin–horseradish peroxidase conjugate (40-fold diluted from stock) was loaded into each well and incubated 20 min at room temperature. After washing, 100 μL of substrate solution (H_2O_2 and tetramethylbenzidine mixture) was loaded into each well and incubated 20 min at room temperature. Finally, 50 μL of stop solution (2 N H_2SO_4) was loaded into each well and thoroughly mixed. Finally, the absorbance of the wells was measured by a microplate reader (Varioskan Flash Spectral Scanning Multimode Reader; Thermo Fisher Scientific) at 450 nm.

ACKNOWLEDGMENTS. Financial support from the National Institutes of Health (Grants U19AI109755 and R01AI117043) is gratefully acknowledged.

1. D. A. Giljohann, C. A. Mirkin, Drivers of biodiagnostic development. *Nature* **462**, 461–464 (2009).
2. M. Urdea *et al*., Requirements for high impact diagnostics in the developing world. *Nature* **444** (suppl. 1), 73–79 (2006).
3. S. O. Kelley *et al*., Advancing the speed, sensitivity and accuracy of biomolecular detection using multi-length-scale engineering. *Nat. Nanotechnol.* **9**, 969–980 (2014).
4. S. O. Kelley, What are clinically relevant levels of cellular and biomolecular analytes? *ACS Sens.* **2**, 193–197 (2017).
5. L. Soleymani, Z. Fang, E. H. Sargent, S. O. Kelley, Programming the detection limits of biosensors through controlled nanostructuring. *Nat. Nanotechnol.* **4**, 844–848 (2009).
6. T. M. Squires, R. J. Messinger, S. R. Manalis, Making it stick: Convection, reaction and diffusion in surface-based biosensors. *Nat. Biotechnol.* **26**, 417–426 (2008).
7. S. Yang, X. Dai, B. B. Stogin, T.-S. Wong, Ultrasensitive surface-enhanced Raman scattering detection in common fluids. *Proc. Natl. Acad. Sci. U.S.A.* **113**, 268–273 (2016).
8. L. Wang, Q. Xiong, F. Xiao, H. Duan, 2D nanomaterials based electrochemical biosensors for cancer diagnosis. *Biosens. Bioelectron.* **89**, 136–151 (2017).
9. Y. Song *et al*., Recent advances in electrochemical biosensors based on graphene two-dimensional nanomaterials. *Biosens. Bioelectron.* **76**, 195–212 (2016).
10. X. Gan, H. Zhao, X. Quan, Two-dimensional MoS_2: A promising building block for biosensors. *Biosens. Bioelectron.* **89**, 56–71 (2017).
11. J.-M. Nam, C. S. Thaxton, C. A. Mirkin, Nanoparticle-based bio-bar codes for the ultrasensitive detection of proteins. *Science* **301**, 1884–1886 (2003).
12. H. D. Hill, C. A. Mirkin, The bio-barcode assay for the detection of protein and nucleic acid targets using DTT-induced ligand exchange. *Nat. Protoc.* **1**, 324–336 (2006).
13. P. M. Kosaka *et al*., Detection of cancer biomarkers in serum using a hybrid mechanical and optoplasmonic nanosensor. *Nat. Nanotechnol.* **9**, 1047–1053 (2014).
14. P. T. K. Loan *et al*., Graphene/MoS_2 heterostructures for ultrasensitive detection of DNA hybridisation. *Adv. Mater.* **26**, 4838–4844 (2014).
15. A. Niemz, T. M. Ferguson, D. S. Boyle, Point-of-care nucleic acid testing for infectious diseases. *Trends Biotechnol.* **29**, 240–250 (2011).
16. J. S. Gootenberg *et al*., Nucleic acid detection with CRISPR-Cas13a/C2c2. *Science* **356**, 438–442 (2017).
17. S. Yang, R. E. Rothman, PCR-based diagnostics for infectious diseases: Uses, limitations, and future applications in acute-care settings. *Lancet Infect. Dis.* **4**, 337–348 (2004).
18. P. Craw, W. Balachandran, Isothermal nucleic acid amplification technologies for point-of-care diagnostics: A critical review. *Lab Chip* **12**, 2469–2486 (2012).
19. C. M. Niemeyer, M. Adler, R. Wacker, Immuno-PCR: High sensitivity detection of proteins by nucleic acid amplification. *Trends Biotechnol.* **23**, 208–216 (2005).
20. R. Bharadwaj, J. G. Santiago, Dynamics of field-amplified sample stacking. *J. Fluid Mech.* **543**, 57–92 (2005).
21. Y. Xu, C.-X. Zhang, D. Janasek, A. Manz, Sub-second isoelectric focusing in free flow using a microfluidic device. *Lab Chip* **3**, 224–227 (2003).
22. R. T. Kelly, A. T. Woolley, Electric field gradient focusing. *J. Sep. Sci.* **28**, 1985–1993 (2005).
23. K. J. Freedman *et al*., Nanopore sensing at ultra-low concentrations using single-molecule dielectrophoretic trapping. *Nat. Commun.* **7**, 10217 (2016).
24. P. Smejkal *et al*., Microfluidic isotachophoresis: A review. *Electrophoresis* **34**, 1493–1509 (2013).
25. Y.-C. Wang, A. L. Stevens, J. Han, Million-fold preconcentration of proteins and peptides by nanofluidic filter. *Anal. Chem.* **77**, 4293–4299 (2005).
26. L. M. Fu, H. H. Hou, P. H. Chiu, R. J. Yang, Sample preconcentration from dilute solutions on micro/nanofluidic platforms: A review. *Electrophoresis* **39**, 289–310 (2018).
27. R. K. Anand, E. Sheridan, D. Hlushkou, U. Tallarek, R. M. Crooks, Bipolar electrode focusing: Tuning the electric field gradient. *Lab Chip* **11**, 518–527 (2011).
28. K. A. Mauritz, R. B. Moore, State of understanding of nafion. *Chem. Rev.* **104**, 4535–4585 (2004).
29. S. J. Kim, Y.-A. Song, J. Han, Nanofluidic concentration devices for biomolecules utilizing ion concentration polarization: Theory, fabrication, and applications. *Chem. Soc. Rev.* **39**, 912–922 (2010).
30. W. Ouyang, X. Ye, Z. Li, J. Han, Deciphering ion concentration polarization-based electrokinetic molecular concentration at the micro-nanofluidic interface: Theoretical limits and scaling laws. *Nanoscale* **10**, 15187–15194 (2018).
31. R. K. Anand, E. Sheridan, K. N. Knust, R. M. Crooks, Bipolar electrode focusing: Faradaic ion concentration polarization. *Anal. Chem.* **83**, 2351–2358 (2011).
32. J. H. Lee, Y.-A. Song, J. Han, Multiplexed proteomic sample preconcentration device using surface-patterned ion-selective membrane. *Lab Chip* **8**, 596–601 (2008).
33. A. Zinkova, I. Brynychova, A. Svacina, M. Jirkovska, M. Korabecna, Cell-free DNA from human plasma and serum differs in content of telomeric sequences and its ability to promote immune response. *Sci. Rep.* **7**, 2591 (2017).
34. M. De *et al*., Sensing of proteins in human serum using conjugates of nanoparticles and green fluorescent protein. *Nat. Chem.* **1**, 461–465 (2009).
35. P. E. Nielsen, *Peptide Nucleic Acids: Protocols and Applications* (Garland Science, 2004).
36. J. Däbritz, J. Hänfler, R. Preston, J. Stieler, H. Oettle, Detection of Ki-ras mutations in tissue and plasma samples of patients with pancreatic cancer using PNA-mediated PCR clamping and hybridisation probes. *Br. J. Cancer* **92**, 405–412 (2005).
37. W. Ouyang, Z. Li, J. Han, Pressure-modulated selective electrokinetic trapping for direct enrichment, purification, and detection of nucleic acids in human serum. *Anal. Chem.* **90**, 11366–11375 (2018).
38. A. Cannas *et al*., *Mycobacterium tuberculosis* DNA detection in soluble fraction of urine from pulmonary tuberculosis patients. *Int. J. Tuberc. Lung Dis.* **12**, 146–151 (2008).
39. V. Masilamani *et al*., Cancer detection by native fluorescence of urine. *J. Biomed. Opt.* **15**, 057003 (2010).
40. R. H. Christenson *et al*., Comparison of 13 commercially available cardiac troponin assays in a multicenter North American study. *J. Appl. Lab. Med.* **1**, 544–561 (2017).
41. T. Omland *et al*.; Prevention of Events with Angiotensin Converting Enzyme Inhibition (PEACE) Trial Investigators, A sensitive cardiac troponin T assay in stable coronary artery disease. *N. Engl. J. Med.* **361**, 2538–2547 (2009).
42. C. Meex *et al*., Direct identification of bacteria from BacT/ALERT anaerobic positive blood cultures by MALDI-TOF MS: MALDI Sepsityper kit versus an in-house saponin method for bacterial extraction. *J. Med. Microbiol.* **61**, 1511–1516 (2012).
43. Z. Pang, N. E. Laplante, R. J. Filkins, Dark pixel intensity determination and its applications in normalizing different exposure time and autofluorescence removal. *J. Microsc.* **246**, 1–10 (2012).